Environ Fluid Mech (2011) 11:385–404
DOI 10.1007/s10652-010-9189-5

ORIGINAL ARTICLE

Undular tidal bores: effect of channel constriction and bridge piers

Hubert Chanson

Received: 11 February 2010 / Accepted: 4 August 2010 / Published online: 20 August 2010

Abstract A tidal bore may occur in a macro-tidal estuary when the tidal range exceeds 4.5–6 m and the estuary bathymetry amplifies the tidal wave. Its upstream propagation induces a strong mixing of the estuarine waters. The propagation of undular tidal bores was investigated herein to study the effect of bridge piers on the bore propagation and characteristics. Both the tidal bore profile and the turbulence generated by the bore were recorded. The free-surface undulation profiles exhibited a quasi-periodic shape, and the potential energy of the undulations represented up to 30% of the potential energy of the tidal bore. The presence of the channel constriction had a major impact on the free-surface properties. The undular tidal bore lost nearly one third of its potential energy per surface area as it propagated through the channel constriction. The detailed instantaneous velocity measurements showed a marked effect of the tidal bore passage suggesting the upstream advection of energetic events and vorticity "clouds" behind the bore front in both channel configurations: prismatic and with constriction. The turbulence patches were linked to some secondary motions and the proposed mechanisms were consistent with some field observations in the Daly River tidal bore. The findings emphasise the strong mixing induced by the tidal bore processes, and the impact of bridge structures on the phenomenon.

Keywords Undular tidal bores · Free-surface undulations · Channel constriction · Bridge piers · Experimental measurements · Turbulent events · Macro-turbulence

1 Introduction

A tidal bore is an unsteady flow motion generated by the rapid water level rise at the river mouth during the early flood tide when the tidal range exceeds 4.5–6 m, the estuary

Electronic supplementary material The online version of this article (doi:10.1007/s10652-010-9189-5) contains supplementary material, which is available to authorized users.

H. Chanson (✉)
Professor in Civil Engineering, The University of Queensland, Brisbane, QLD 4072, Australia
e-mail: h.chanson@uq.edu.au

Fig. 1 Undular tidal bore of the Dordogne River (France) on 27 September 2008 at 15:50—the two kayakers were riding the second wave and Fabrice COLAS was surfing on the third wave

bathymetry amplifies the tidal wave and the freshwater level is low. As the tidal level in the estuary rises with time during the early flood tide, the leading edge of the tide, called the tidal wave, becomes steeper and steeper until it forms an abrupt front that is the tidal bore [24,28] (Fig. 1). On our planet, the tidal bores occur widely in macro-tidal estuaries and rivers. They exert a major impact on the ecology and environment of estuarine zones in particular in the transport of sediments and the reproduction of some native fish species [8,11,30,31].

Historically, some major contributions on tidal bores encompassed [1,2,24] and [28]. A limited number of field investigations were conducted, including by Kjerfve and Ferreira [20] and Wolanski et al. [35]. More recently, some unsteady turbulence measurements were conducted using PIV and ADV techniques [7,19,21] (Table 1). These physical data highlighted the intense turbulence generated during the tidal bore propagation. Some numerical modelling presented some interesting features [15,23,26], but the comparison with physical data showed some limitations.

The impact of a tidal bore on a bridge as well as the effect of the bridge on the tidal bore process were rarely documented although some studies were conducted on the impact of the Hangzhou Bay bridge (China) opened in 2008. Another example is the 15th century bridge, called Pont Aubaud, across the Sélune River in France. Figure 2 illustrates the propagation of an undular tidal bore underneath. Note the bridge piers shaped to cut the tidal bore flow (Fig. 2).

To date there is basically no information on the impact of bridge structures and channel constructions on tidal bores and the associated impact in terms of mixing. The present contribution examines in detail the propagation of undular tidal bores between piers, the turbulence and turbulent mixing generated by the passage of the bore in the short channel constriction and the impact of the bridge on the tidal bore. The experimental results show the major impact of the short transition on the tidal bore motion. The paper is further supported by a online appendix presenting some movies.

Table 1 Experimental flow conditions

Reference	S_0	Q	d_0	Gate opening h	Surge type at x = 5 m	U	Fr	Remarks
		(m^3/s)	(m)	(m)		(m/s)		
(1)	(2)	(3)	(4)	(5)	(6)	(7)	(8)	(9)
Hornung et al. [19]	0	0	–	N/A	Undular to breaking	–	1.5–6	Smooth bed L = 24 m
Koch and Chanson [21]	0	0.040	0.079	0.010–0.092	Undular to breaking	0.14–0.68	1.31–1.93	Smooth PVC bed. L = 12 m, B = 0.5 m
Chanson [7]								
Series 1A	0	0.058	0.137	0.010–0.110	Undular to breaking	0.56–0.90	1.17–1.49	Smooth PVC bed. L = 12 m, B = 0.5 m
Series 1B	0	0.058	0.142*	0.010–0.105	Undular to breaking	0.50–0.89	1.13–1.47	Rough screens (k = 8 mm). L = 12 m, B = 0.5 m
Present study								Smooth PVC bed. L = 12 m, B = 0.5 m
Series 1	0	0.0089–0.0511	0.056–0.212	0–0.07	Undular to breaking	0.67–1.37	1.04–1.95	Free-surface measurements. Runs 090122_01–090423_803
Series 2	0	0.0188–0.0190	0.115–0.199	0	Undular	1.05– 1.32	1.08–1.16	Turbulence measurements

Notes: d_0: initial depth measured at x = 5 m in absence of constriction or x = 3.6 m with channel constriction; Fr: tidal bore Froude number $\left(\mathrm{Fr} = (V_0 + U)/\sqrt{g \times d_0}\right)$; h: tainter gate opening after closure; Q: initial steady flow rate; U: bore front celerity measured at x = 5 m in absence of constriction or x = 3.6 m with channel constriction; * above rough screens

Fig. 2 Propagation of the Sélune River tidal bore beneath the Pont Aubault (France) on 7 April 2004 at 09:00—view from the left bank

2 Experimental setup and instrumentation

The experiments were performed in a 12 m long, 0.5 m wide tilting flume, and its slope was set horizontal for all experiments. The flume was made of smooth PVC bed and glass walls. The initial flow conditions were controlled by a radial gate located at the channel downstream end (x = 11.9 m) while the tidal bore generation was induced by the rapid closure of a tainter gate which was located next to and just upstream of the radial gate. The tainter gate closure time was between 0.1 and 0.15 s.

The water discharge was measured with two orifice meters. In steady flows, the water depths were measured using rail mounted pointer gauges, and the unsteady water depths were measured with a series of acoustic displacement meters Microsonic^{TM} Mic+25/IU/TC unit located at several longitudinal distances along the channel centreline. The turbulent velocity measurements were conducted with an acoustic Doppler velocimeter Nortek^{TM} Vectrino+ (Serial No. VNO 0436) equipped with a three-dimensional side-looking head. The sampling rate was 200 Hz and the velocity data accuracy was 1% of the velocity range (0.3 or 1 m/s herein). The acoustic displacement meters and acoustic Doppler velocimeter were synchronised within 1 ms, and were sampled simultaneously. The translation of the ADV probe in the vertical direction was controlled by a fine adjustment travelling mechanism connected to a Mitutoyo^{TM} digimatic scale unit. The error on the vertical position of the probe was $\Delta z < 0.025$ mm.

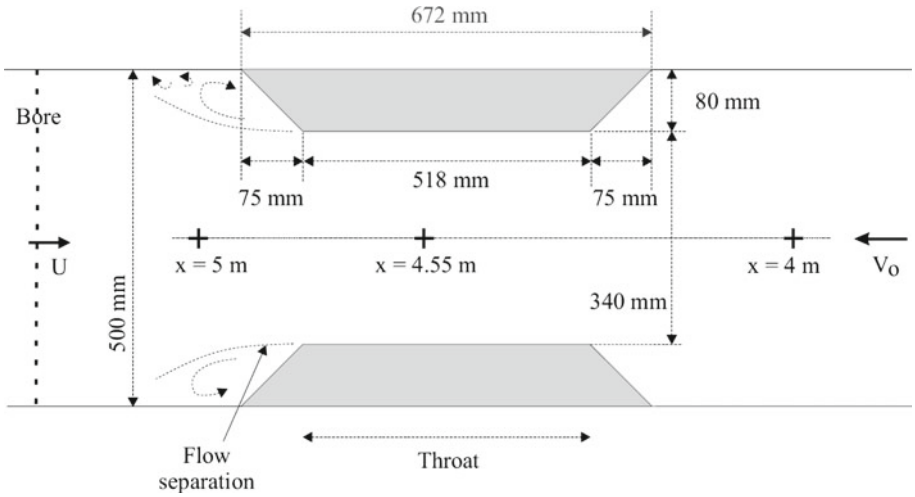

Fig. 3 Experimental channel and constriction installation in the rectangular channel: dimensioned sketch

The experimental flow conditions are summarised in Table 1. Further information on the facility and instrumentation is reported in Chanson [5] including some movies of the experiments.

2.1 Channel constriction

For some experiments, a channel constriction was introduced as shown in Fig. 3 where x is the longitudinal distance from the channel upstream end. Both sides were identical, made of mortar and painted. Note that the channel constriction was typical of a set of bridge piers, being a 1:20 scale model of the Pont Aubault bridge (Fig. 2). In steady flow conditions, the visual observations showed the presence of shock waves/cross-waves between the half-bridge piers when the upstream Froude number $Fr_0 = V_0/\sqrt{g \times d_0}$ was larger than 0.2 where V_0 and d_0 are respectively the flow velocity and depth measured upstream of the constriction. For $Fr_0 < 0.2$, only small ripples were seen in the channel constriction. For all investigations, the initially steady flow was characterised by some flow separation downstream of the constriction as sketched in Fig. 3: i.e., with a jet flow region along the channel centreline where the steady flow measurements showed some larger centreline velocities.

2.2 ADV signal processing and analysis

The ADV system records the three instantaneous velocity components at high frequency (200 Hz herein). The present experience demonstrated some recurrent issues, including low correlations and low signal to noise ratios, when the waters were not seeded [5]. The situation improved drastically by a combination of measures, including the injection of kaolin powder and some stirring in the intake chamber prior to each run.

In steady flows, the signal processing removed all the samples with communication errors, average correlation below 60% or signal-to-noise ratio (SNR) below 5 dB, and the data were "despiked" using a phase-space thresholding technique [9,16,34]. The ADV post-processing techniques were devised for steady flows, and these are not applicable to unsteady flows.

Herein the unsteady flow post-processing was limited to a removal of communication errors following Koch and Chanson [21].

3 Basic flow patterns

In the prismatic channel, two basic flow patterns were observed depending upon the bore Froude number $Fr = (V_0 + U)/\sqrt{g \times d_0}$ where d_0 is the initial flow depth, V_0 is the initial flow velocity positive downstream, g is the gravity acceleration and U is the surge front celerity for an observer standing on the bank, positive upstream. The tidal bore was undular for a Froude number less than 1.5–1.6 and a breaking bore for larger bore Froude numbers. For Fr < 1.5–1.6, the tidal bore front was followed a train of well-formed, quasi-periodic undulations. For Fr > 1.5–1.6, the bore front had a marked roller associated with some air entrainment and turbulent mixing. For the entire range of investigations, the basic flow patterns were consistent with the earlier findings of Favre [14], Hornung et al. [19] and Koch and Chanson [21].

The effects of the channel constriction were documented for a range of flow conditions corresponding to an initially steady subcritical flow ($0.12 \leq Fr_0 \leq 0.31$) and the upstream propagation of undular tidal bores (Table 1). Figure 4 illustrates the propagation of an undular bore (Fr = 1.23) in the channel constriction, looking upstream. Each photograph was taken 0.5 s apart. A number of short movies are available in the digital appendix. The visual observations showed that the entrance of the bore into the converging constriction was associated with some reflection propagating back towards the channel downstream end, together with the development of a turbulent free-surface motion in the throat (Fig. 2, 4, 5 and 6). As the tidal bore progressed into the constriction, the free-surface exhibited some strongly three-dimensional pattern. When the bore exited the constriction, it tended to regain its quasi-two-dimensional appearance about 0.75–1.5 m after the diverging constriction. It is presently unknown why the undular bore regained so rapidly its two-dimensional profile. This might be linked to the properties of positive surges and tidal bores to absorb any random disturbances that may exist at the free-surface in front of and behind the bore front [4,17]. It is also a well-known observation in the field.

The shock reflection on the converging constriction was associated with the development of surface scars that illustrated the existence of some large turbulent structures next to the free-surface. Figure 5 shows some surface scar development as the bore front advanced in the throat. The bore propagation through the constriction was further linked to some free-surface turbulence and pseudo-chaotic surface motion in the throat. These were possibly best observed using the light glare and reflection at the free-surface. Some surface turbulence was observed also next to the exit/divergent (i.e. upstream end of the channel constriction) in the wake of the sidewall expansions (Fig. 6). Figure 6 illustrates the turbulent vortices delimited by the surface scars as the undular bore front (first wave crest) exited the constriction. It is acknowledged that the sidewalls might adversely impact the development of large-scale structures in the present study. Herein the sidewalls acted as some planes of symmetry but would prevent the development large coherent structures reflected at the downstream end of a whole bridge pier.

Altogether the propagation of the bore through the short channel constriction was associated with the development of large-scale free-surface turbulence and some turbulent dissipation, while the tidal bore regained its quasi-two-dimensional flow pattern further upstream.

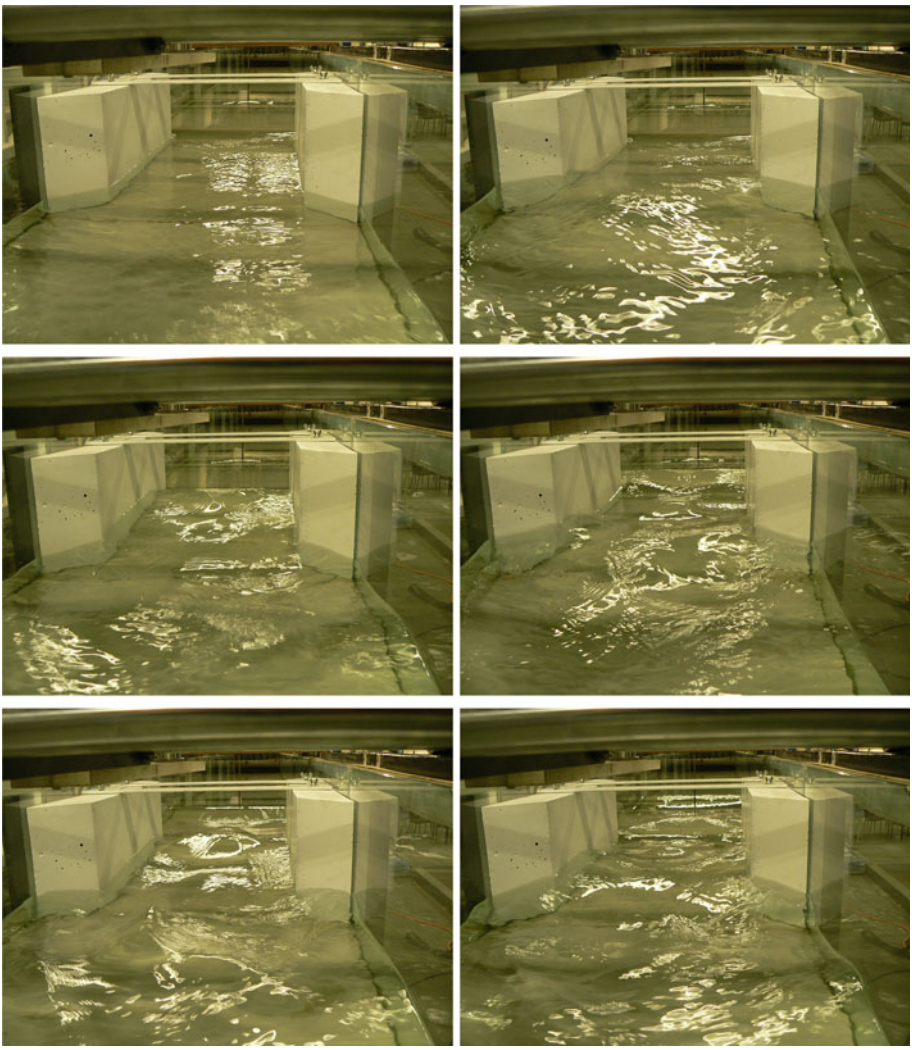

Fig. 4 Undular tidal bore propagation in the constriction, looking upstream—Note the free-surface turbulence in the foreground caused by some reflection as well as the three-dimensional nature of the flow in the throat—from *left* to *right*, *top* to *bottom*: $t = t_0$, $t_0 + 0.5$ s, $t_0 + 1$ s, $t_0 + 1.5$ s, $t_0 + 2$ s, $t_0 + 2.5$ s, Shutter speed: 1/40 s—run 090324_00, $Q = 0.0097$ m^3/s, $d_0 = 0.0882$ mm (at x = 3.6 m), Fr = 1.23, U = 0.885 m/s

4 Free-surface properties of undular tidal bores

The channel constriction had a significant effect on the undular tidal bore propagation and its free-surface profile as illustrated in Fig. 7. Figure 7 shows some time-series of the dimensionless flow depth d/d_0 on the channel centreline at several longitudinal locations when an experiment was repeated with the prismatic channel (Fig. 7a) and in presence of the channel constriction (Fig. 7b).

First the comparative analysis of the data showed the smooth, quasi-periodic undular pattern in the prismatic channel (Fig. 7a), and the energetic and somehow chaotic wave motion in the throat of the channel constriction at x = 4.55 m in Fig. 7b. The centreline

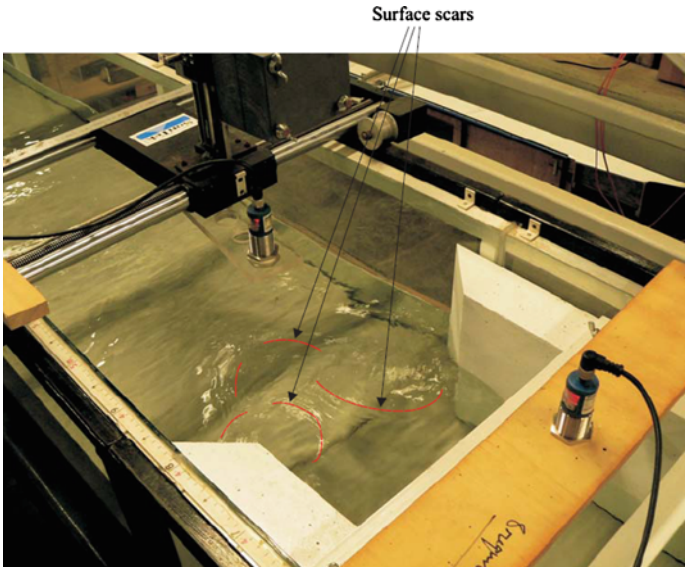

Fig. 5 Undular tidal bore, looking at the first wave crest entering the constriction—note the free-surface turbulence and scars next to the throat convergent—shutter speed: 1/50 s—run 090415_61, Q = 0.0089 m^3/s, d_0 = 0.0845 mm (at x = 3.6 m), Fr = 1.16, U = 0.85 m/s

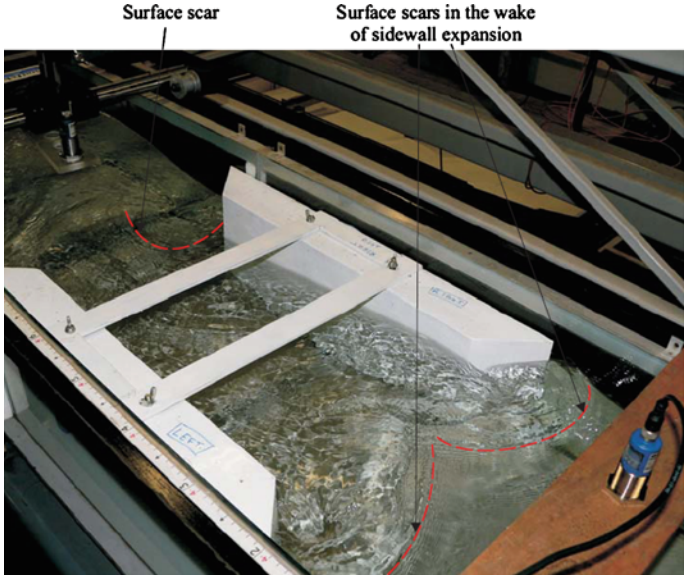

Fig. 6 First wave crest of the undular bore (Fr = 1.15) exiting the channel constriction—note the complicated turbulent pattern upstream of the channel constriction (right) as well as the surface scars in the throat and in the diverging constriction—bore propagation from *top left* to *bottom right*, Shutter speed: 1/80 s–run 090318_00, Q = 0.0232 m^3/s, d_0 = 0.1552 mm (at x = 3.6 m), Fr = 1.15, U = 1.10 m/s

data were consistent with the visual observations, and tended to show a greater maximum wave height in the constriction throat (Fig. 7b, x = 4.55 m). Second, some key differences were seen in the free-surface profiles at x = 5 and 4 m, respectively just before and just

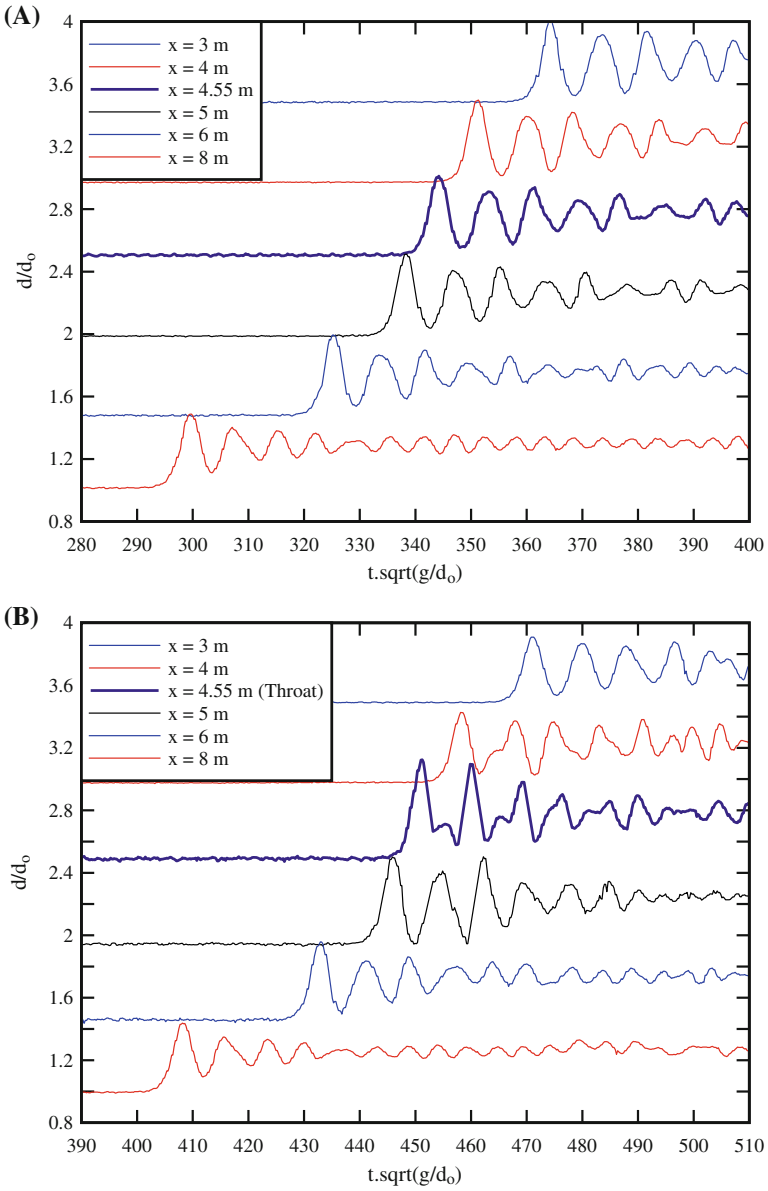

Fig. 7 Dimensionless time-variations of the flow depth during the propagation of an undular tidal bore with and without bridge pier model: Q = 0.0089 m^3/s, d_0 = 0.08 m, Fr = 1.16–1.22, U = 0.8 m/s—each curve was offset vertically by 0.5. **a** No channel constriction—run 090417_62, Q = 0.0089 m^3/s, d_0 = 0.0802 m, Fr = 1.22, U = 0.862 m/s. **b** With channel constriction—run 090417_61, Q = 0.0089 m^3/s, d_0 = 0.0845 m, Fr = 1.16, U = 0.847 m/s

after the constriction. These highlighted some effects of the channel contraction and expansion respectively on the tidal bore propagation. Visually, some wave reflection process was observed downstream of the constriction (i.e. x > 4.9 m), while at x = 4 m, the rapid channel expansion induced a rapid change in free-surface profile. Third, the data in the throat

(x = 4.55 m) showed some form of secondary peak possibly caused by some reflection effect on the walls (Fig. 7b).

The wave energy of the free-surface undulations is a combination of (a) the potential energy due to the water the elevation above the mean water level, and (b) the kinetic energy due to the fluid motion. Over one wave length, the potential energy is equal to the integral of the weight of water above the mean water level times the distance to the centroid:

$$\text{P.E.} = \int_0^{L_w} \frac{1}{2} \times \rho \times g \times \eta^2 \times B \times dx \tag{1}$$

where η is the water elevation relative to the mean water level over the wave length L_w and B is the channel width [25]. Note that Eq. 1 implies a two-dimensional wave propagation. In undular tidal bores, the classical linear wave theory results are not valid because the wave shape is non-linear; the velocity distributions are complex and the kinetic energy cannot be analytically deduced. Instead the potential energy was calculated and used herein as a surrogate of the total energy. Since the water elevation was recorded as a function of time at a fixed location, the potential energy over a wave period T may be deduced by changing the variables from space to time:

$$\text{P.E.} = \int_0^{T} \frac{1}{2} \times \rho \times g \times \eta^2 \times U \times B \times dt \tag{2}$$

where U is the bore celerity. Note that the water elevation η was calculated relative to the average water level over the wave length L_w defined herein from a wave crest to the next wave crest. Figure 8 illustrates the integration process. The potential energy per unit surface area is then:

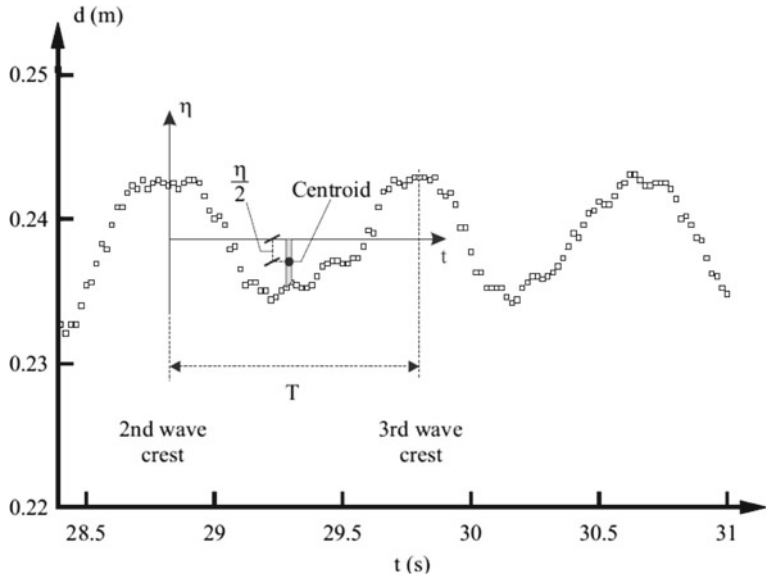

Fig. 8 Potential energy integration along the second wave length—experimental data: Run 090417_63, x = 5 m, Q = 0.0190 m^3/s, d_0 = 0.212 m at x = 3.6 m, Fr = 1.04, U = 1.32 m/s

$$E_p = \frac{\text{P.E.}}{U \times T \times B} = \frac{1}{T} \times \int_0^T \frac{1}{2} \times \rho \times g \times \eta^2 \times dt \tag{3}$$

Typical experimental results are presented in Fig. 9, where the dimensionless potential energy per unit area $E_p/(0.5 \times \rho \times g \times d_0^2)$ is plotted as a function of the dimensionless distance x/d_0. Fig 9a presents some data in the prismatic channel and Fig 9b shows some results with the channel constriction. The data showed typically an increasing potential energy with increasing distance from the gate ($x/d_0 \approx 135$ in Fig 9) down to x = 6 m ($x/d_0 \approx 75$ in Fig. 9). This corresponded to the formation and development of the bore, and the visual observations suggested that the tidal bore profile was nearly invariant with distance for x < 6 m ($x/d_0 < 70$ in Fig. 9). For x < 6 m, the potential energy of the undulations were thereaf-

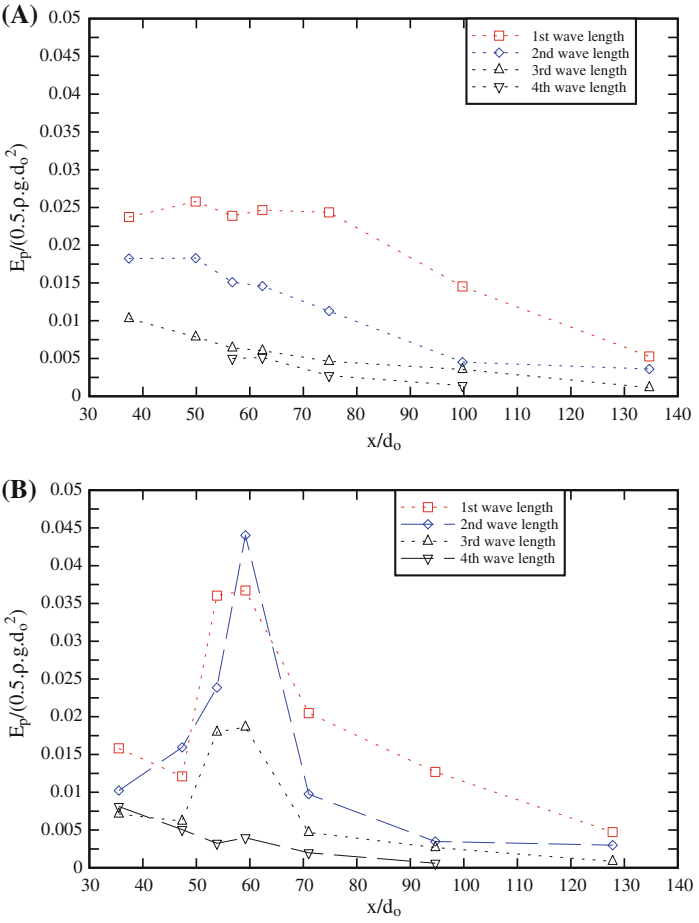

Fig. 9 Dimensionless potential energy per surface area in an undular bore with and without channel constriction—experimental data: Q = 0.0089 m^3/s, d_0 = 0.08 m at x = 3.6 m, Fr = 1.2, U = 0.85 m/s. **a** No constriction—experimental data: Run 090415_62, Q = 0.089 m^3/s, d_0 = 0.0802 m at x = 3.6 m, Fr = 1.22, U = 0.862 m/s. **b** With channel constriction ($47.3 < x/d_0 < 54.8$)—experimental data: run 090415_61, Q = 0.089 m^3/s, d_0 = 0.0845 m at x = 3.6 m, Fr = 1.16, U = 0.847 m/s

ter quasi-constant in absence of channel constriction. The data highlighted further a greater potential energy per unit area in the first wave length than in the subsequent wave lengths (Fig. 9a).

In presence of the channel constriction, the experimental data showed a marked increase in potential energy in the constriction throat: e.g., for $47.3 < x/d_0 < 54.8$ in Fig. 9b. The data indicated also a larger potential energy per surface area immediately upstream of the convergent and downstream of the divergent. This trend is clearly seen in Fig. 9b for the first three wave lengths. It corresponded to some effects of the bore reflection on the convergent as well as of the divergent of the channel constriction. After the channel constriction (i.e. $x/d_0 < 40$), the data suggested a lesser potential energy of the free-surface undulations than in the experiments without constriction (Fig. 9). The potential energy per unit surface area E_p was about 1/3rd smaller after the bore propagation through the channel constriction than for the same bore in a prismatic rectangular channel without constriction (Fig. 9a).

Another quantitative information is the total potential energy per surface area of the tidal bore estimated as:

$$(E_p)_{bore} = \frac{1}{T} \times \int_0^T \frac{1}{2} \times \rho \times g \times (d - d_0)^2 \times dt \tag{4}$$

In the present study, the potential energy of the undulations represented up to 30% of the total potential energy of the tidal bore, and this ratio decreased with an increasing wave length number (Fig. 10). The largest ratio of potential energy of the undulations to the total potential energy of the bore was observed for $Fr \approx 1.3$ which corresponded to the onset of wave breaking at the first wave crest. Typical data are presented in Fig. 10.

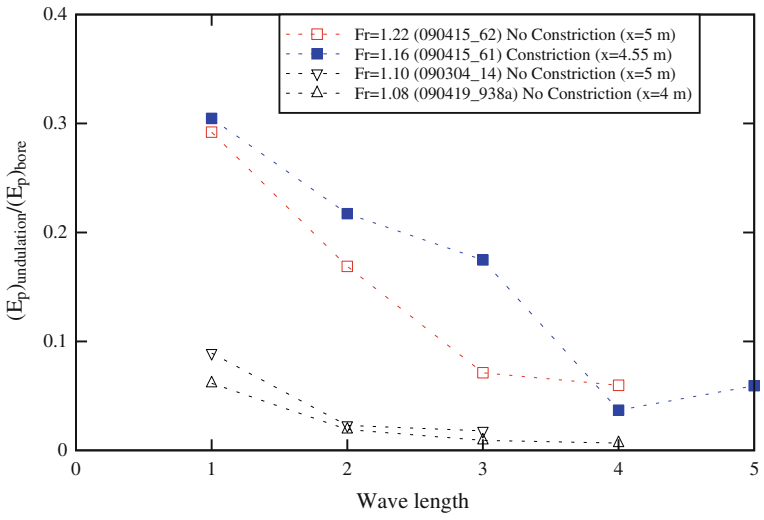

Fig. 10 Ratio of the potential energy of the undulations to the bore potential energy as a function of the wave length number

5 Turbulent velocity measurements

The turbulent velocity measurements were conducted with an initial flow rate $Q = 0.019\ m^3/s$, but different initial flow depths ($0.115 < d_0 < 0.199$ m). The measurements were performed at x = 4, 4.55 and 5 m located respectively upstream, in the middle and downstream of the channel constriction (Fig. 3). A key feature was the repetition of identical experiments without and with the channel constriction, keeping the same identical initial flow conditions (Table 1).

In the prismatic channel, the undular bore was characterised by a smooth first wave crest followed by a series of free-surface undulations. When the undular bore front passed above

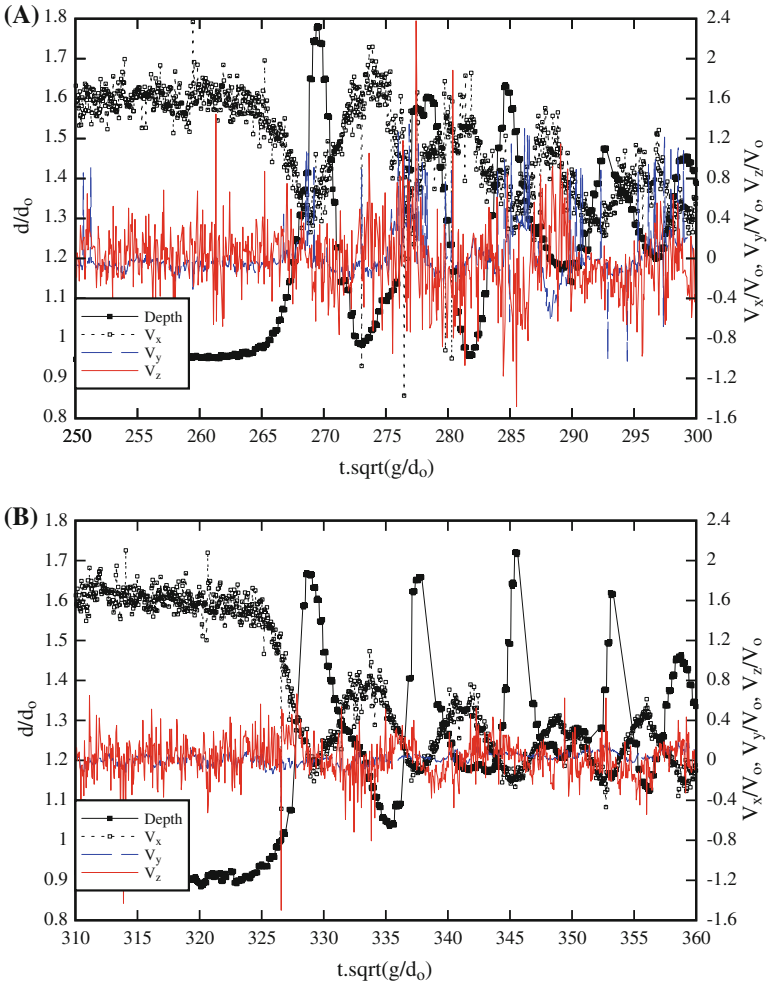

Fig. 11 Dimensionless water depth and instantaneous velocity components in an undular bore propagating upstream in a channel with channel constriction—run 090424_901-906, $d_0 = 0.1147$ m at x = 3.6 m, $V_0 = 0.3313$ m/s, U = 1.05 m/s, Fr = 1.16. **a** Downstream of constriction: x = 5 m, $z/d_0 = 0.312$, run 090424_901c. **b** In the constriction throat: x = 4.55 m, $z/d_0 = 0.312$, run 090424_903. **c** Upstream of the constriction: x = 4 m, $z/d_0 = 0.316$, run 090424_905

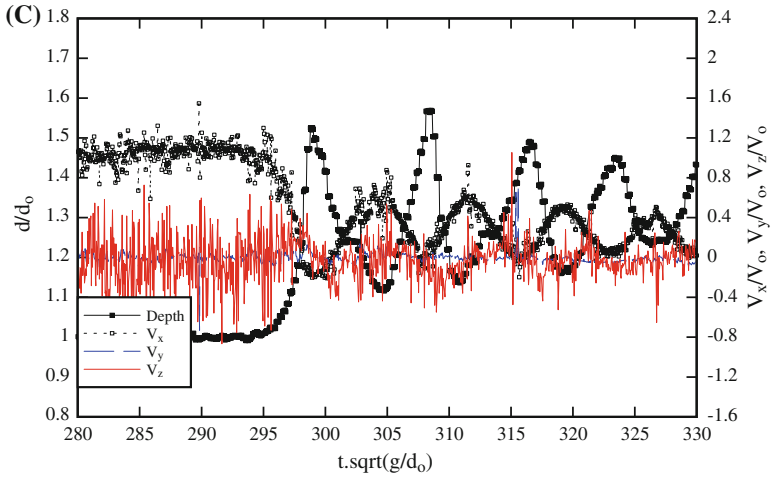

Fig. 11 continued

the sampling volume, a relatively gentle longitudinal flow deceleration was observed at all vertical elevations. The longitudinal velocity component was minimum beneath the first wave crest and it oscillated afterwards with the same period as the surface undulations and out of phase as previously observed by Koch and Chanson [21] and Chanson [7] in laboratory, and Wolanski et al. [35] in the Daly River. The longitudinal velocities were maximum beneath the wave troughs and minimum below the wave crests at all sampling elevations. Close to the free-surface, the vertical velocity data presented also some oscillating pattern. The basic flow net theory predicts these redistributions in longitudinal and vertical velocity components since the free-surface is a streamline [6,27,29].

Figure 11 presents some typical dimensionless depth d/d_0 and velocity components V_x/V_0, V_y/V_0 and V_z/V_0 in presence of the channel constriction. These data were collected at the same vertical elevation z/d_0 on the channel centreline, and the three sampling locations are drawn to scale in Fig. 3. The velocity measurements suggested small to moderate effects of the channel constriction on the unsteady turbulent velocity field. The finding was somehow deceiving since a significant impact of the constriction was observed visually and measured in terms of the free-surface profile. However the data sets suggested some energetic turbulent events beneath the first and subsequent wave lengths. These were best seen by some sudden and rapid fluctuations of the transverse velocity data V_y/V_0 as highlighted in Fig. 12. Such vigorous turbulent events were also observed in the prismatic rectangular channel in both the present and past studies [7,21]. The present study suggested however some more intense occurrence in and next to the channel constriction.

6 Discussion

It is argued herein that the energetic turbulent events illustrated in Fig. 12 were some form of "macro-turbulence", or large-scale turbulence, produced beneath the tidal bore front and advected upstream behind the tidal bore, that were likely induced by secondary motion. The evidences of advected turbulent "patches" behind a tidal bore were documented in the field: e.g., in the Mersey River (UK) and Rio Mearim (Brazil) [12,20]; in the Daly River (Aus-

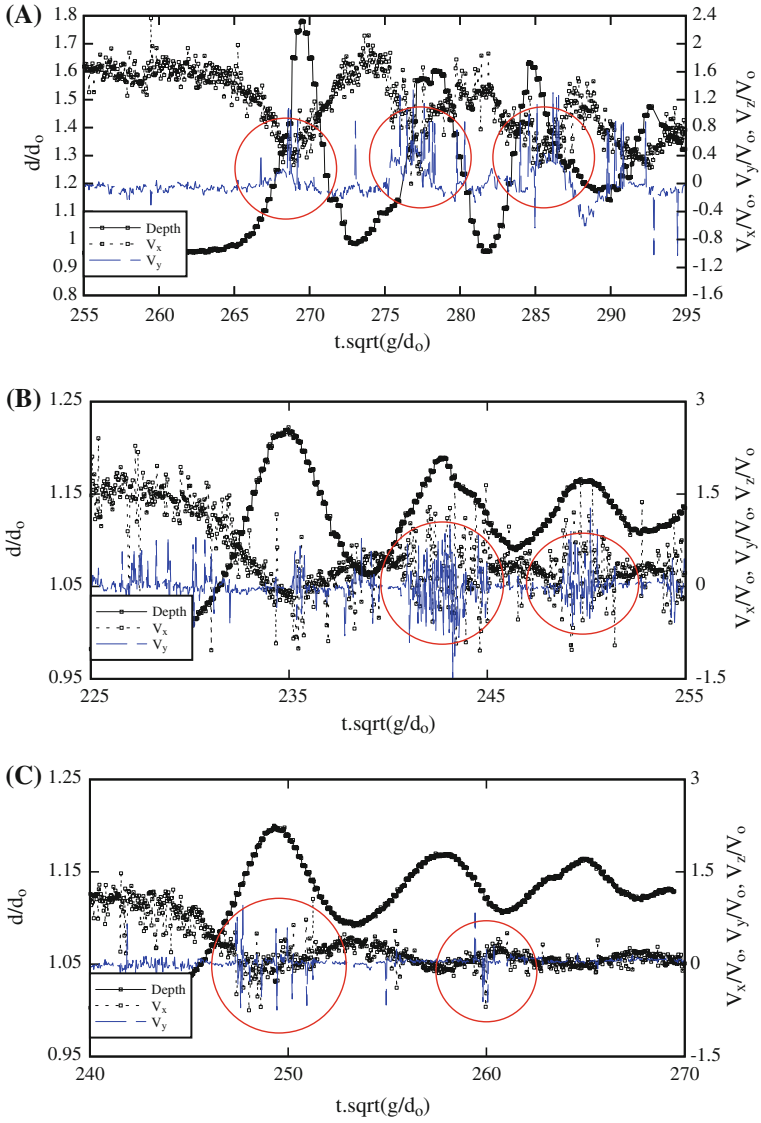

Fig. 12 Turbulent events behind tidal bores in a channel with channel constriction: dimensionless water depth and instantaneous longitudinal and transverse velocity components. **a** Downstream of constriction: x = 5 m, $z/d_0 = 0.312$, run 090424_901c, $d_0 = 0.1147$ m at x = 3.6 m, $V_0 = 0.3313$ m/s, U = 1.05 m/s, Fr = 1.16. **b** In the constriction throat: x = 4.55 m, $z/d_0 = 0.73$, run 090429_934, $d_0 = 0.1989$ m at x = 3.6 m, $V_0 = 0.189$ m/s, U = 1.32 m/s, Fr = 1.08. **c** Upstream of the constriction: x = 4 m, $z/d_0 = 0.182$, run 090429_935, $d_0 = 0.1989$ m at x = 3.6 m, $V_0 = 0.189$ m/s, U = 1.32 m/s, Fr = 1.08

tralia) and the northern Branch of the Changjiang River estuary [10,35]. In these estuaries, some delayed jumps in salinity, temperature and suspended sediment concentration implied some turbulent advection process in the wake of the tidal bore. An unusual observation was recorded in the Daly River (Australia) where a period of very strong turbulence was observed about twenty minutes after the bore passage that lasted for about 3 min [35]. In that study, the

sampling location was located about 50 km upstream of the river mouth, and the anecdote suggested the upstream advection of a "cloud" of turbulence and vorticity for a considerable distance.

In the present study, the instantaneous velocity data showed some large fluctuations in transverse velocities V_y on the channel centreline (Fig. 12). The findings highlighted the existence of transient secondary currents behind the bore front. These intense turbulent events were observed at several longitudinal locations highlighting the upstream advection process. While these turbulent bursts might be linked to the undular shape of the bore, Hornung et al. [19] and Koch and Chanson [22] presented some evidences of turbulence "patches" behind both undular and breaking bores, with a vorticity production rate proportional to $(Fr - 1)^3$. These studies implied that the vorticity "clouds" were a feature of both non-breaking and breaking bores, and the finding was supported by some recent numerical results [15,26]. The present results suggested further that some turbulence clouds could be linked to the non-prismatic channel shape, and hence with some secondary current motion.

The secondary currents are currents that develop in the plane normal to the local axis of the main flow. In a prismatic channel, the vorticity profiles at the sidewall and on the invert interact next to the corner (Fig. 13, Inset). As a result, there exists a mean flow in the y-z-plane that corresponds to the secondary current sketched in Fig. 13. This secondary motion is driven by the Reynolds stress gradients [3]. The secondary currents may also occur in the regions of transition from smooth to rough boundaries when the boundary roughness is not uniform as shown by Hinze [18]. Considering a tidal bore propagating upstream in a prismatic rectangular channel, it induced some intense turbulent mixing, and it hypothesised that some strong turbulent kinetic energy production caused by secondary motion next to the step corners took place beneath the wave troughs, as sketched in Fig. 13. The turbulent events interacted with the mean flow and some energetic "clouds" of turbulence were advected within the main flow behind the bore. Figure 14 presents some tangential stress data recorded in the channel centreline; the data corresponded to the velocity data presented in Fig. 12a downstream of the channel constriction. The Reynolds stress data showed the large magnitude and fluctuations of the turbulent stresses beneath the undulations at all vertical elevations. The Reynolds stress magnitudes were larger beneath the undulations than in the initially steady flow, and they were significant during the macro-turbulence "patches".

When the channel is not prismatic, there is a change in mean flow direction and the streamline curvature induces some longitudinal component of mean vorticity. Some vorticity may be generated by the inviscid flow motion and some complicated secondary currents may develop [32,33,36]. In the present study, the tidal propagation in the channel constriction was associated with the development of large scale vortical structures next to the free-surface at the throat intake and in the divergent section (Fig. 5 and 6). It is believed that the free-surface boil structures illustrated the intense production of turbulent kinetic energy and vorticity next to the sidewall contraction and expansion when the bore front entered and exited respectively the constriction. The macro-scale turbulence was advected behind the bore front, contributing to the energetic turbulent velocity fluctuation periods observed on the channel centreline (Fig. 12). The proposed mechanism would be consistent with the surface "*clockwise and counterclockwise rotating eddies*", "*quasi two dimensional, rotating around a vertical axis*", observed in the Daly River by Wolanski et al. [35] about 20 min after the tidal bore passage.

Some transient fronts were also observed behind some tidal bores and they can induce further secondary currents and vertical circulation. The author saw several examples of transient fronts behind tidal bores in the Baie du Mont Saint Michel; in each case, the transient front arrived a couple of minutes after the bore front and lasted several minutes.

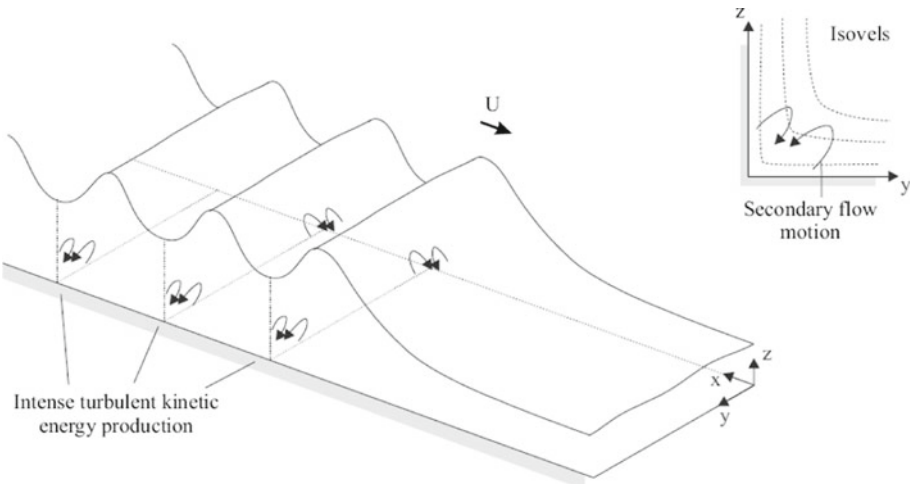

Fig. 13 Secondary currents in an undular bore propagating in a prismatic channel—*inset*: secondary flow motion in a corner

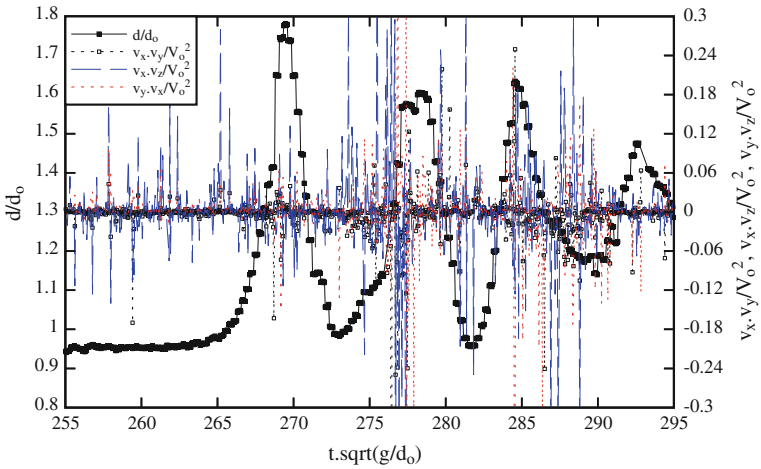

Fig. 14 Dimensionless water depth and tangential stresses in an undular bore in a rectangular channel—downstream of constriction: x = 5 m, $z/d_0 = 0.312$, run 090424_901c, $d_0 = 0.1147$ m at x = 3.6 m, $V_0 = 0.3313$ m/s, U = 1.05 m/s, Fr = 1.16

Secondary flows associated with such fronts can lead to enhanced scalar concentrations of larvae and pollutants, and enhanced sediment transport [13]. Their presence influences the horizontal dispersion and residual circulation in the flood flow.

7 Conclusion

The tidal bores are observed when the tidal flow turns to rising in macro-tidal estuaries and the estuarine bathymetry is funnel-shaped to amplify the tidal wave. Herein a new experimental investigation was conducted in a rectangular channel with and without a constriction. Some detailed velocity measurements were performed in the undular tidal bores

with a high temporal and spatial resolution while the free-surface elevations were recorded using non-intrusive sensors. The experiments were designed to study the effects of bridge piers on the undular tidal bores.

The free-surface undulation profiles exhibited a quasi-periodic shape. An analysis of the potential energy showed that the potential energy of the free-surface undulations represented up to 30% of the potential energy of the undular tidal bore. The presence of a channel constriction had a major impact on the free-surface properties. In the channel throat, the wave motion was three-dimensional, pseudo-chaotic and energetic. Some shock reflection in the channel convergent was associated with the development of large-scale vortical structures at the free-surface. In the divergent section, some large free-surface scars were observed highlighting some intense turbulence production in the wake of the sidewall expansion. The undular tidal bore lost nearly one third of its potential energy per surface area, on average for all flow conditions, as it propagated through the channel constriction.

The instantaneous velocity measurements showed a marked effect of the tidal bore passage in a prismatic channel. The streamwise velocities were characterised by some flow deceleration at all vertical elevations, and some large fluctuations of all velocity components were recorded beneath the bore and undulations. The velocity measurements showed some small to moderate effects of the channel constriction on the unsteady turbulent velocity field. However the velocity data sets suggested the upstream advection of energetic events and vorticity "clouds" behind the bore front in both channel configurations: prismatic and with constriction. This was seen in particular by some sudden and rapid fluctuations of the transverse velocity data V_y/V_0. It is suggested that the energetic turbulent events were some form of macro-turbulence generated by transient secondary motion and advected upstream behind the bore. In presence of a channel constriction, some strong macro-scale turbulence was produced additionally as the tidal bore propagated through the constriction, and further vorticity was produced and later advected behind the bore front. The proposed mechanisms were consistent with some field observations in the Daly River tidal bore and recent numerical simulations.

Overall the study findings showed that a constriction typical of bridge piers had a significant impact on tidal bore characteristics including their mixing properties.

Acknowledgements The author acknowledges the technical assistance of Graham ILLIDGE and Clive BOOTH (The University of Queensland). He thanks Dr Dominique MOUAZÉ (University of Caen, France) for his helpful comments. Further the author thanks the two anonymous reviewers for their useful comments.

References

1. Barré de Saint-Venant AJC (1871) Théorie et Equations Générales du Mouvement Non Permanent des Eaux Courantes. In: Comptes Rendus des séances de l'Académie des Sciences, vol 73, Paris, France, Séance 17 July 1871, pp 147–154 (in French)
2. Bazin H (1865) Recherches Expérimentales sur la Propagation des Ondes. (Experimental Research on Wave Propagation). In: Mémoires présentés par divers savants à l'Académie des Sciences, vol 19, Paris, France, 495–644 (in French)
3. Bradshaw P (1971) An Introduction to Turbulence and its Measurement. Pergamon Press, Oxford, UK, 218 pp (The Commonwealth and International Library of Science and technology Engineering and Liberal Studies, Thermodynamics and Fluid Mechanics Division)
4. Chanson H (2004) The hydraulics of open channel flow: an introduction, 2nd edn. Butterworth-Heinemann, Oxford, UK, 630 pp
5. Chanson H (2009) An experimental study of tidal bore propagation: the impact of bridge piers and channel constriction. Hydraulic model report no. CH74/09, School of Civil Engineering, The University of Queensland, Brisbane, Australia, 110 pp (5 movies)

6. Chanson H (2009) Applied hydrodynamics: an introduction to ideal and real fluid flows. CRC Press/ Balkema, Taylor & Francis Group, Leiden, The Netherlands, 478 pp
7. Chanson H (2010) Unsteady turbulence in tidal bores: effects of bed roughness. J Waterway Port Coastal Ocean Eng ASCE 136(5):247–256
8. Chanson H, Tan KK (2011) Turbulent mixing of particles under tidal bores: an experimental analysis. J Hydraul Res, IAHR 49 (in press)
9. Chanson H, Trevethan M, Aoki S (2008) Acoustic doppler velocimetry (ADV) in small estuary : field experience and signal post-processing. Flow Meas Instrum 19(5):307–313. doi:10.1016/j.flowmeasinst.2008.03.003
10. Chen S (2003) Tidal bore in the north branch of the Changjiang estuary. In: Proceedings of international conference on estuaries & coasts ICEC-2003, vol 1, Hangzhou, China, November 8–11, International Research & Training Center on Erosion & Sedimentation Ed., pp 233–239
11. Chen J, Liu C, Zhang C, Walker HJ (1990) Geomorphological development and sedimentation in Qiantang estuary and Hangzhou bay. J Coastal Res 6(3):559–572
12. Davies C (1988) Tidal river bores. Dissertation in partial fulfilment of B.A. degree, Department of Geography, Edge Hill College, University of Lancaster, UK
13. Dyer KR (1997) Estuaries. A physical introduction, 2nd edn. Wiley, New York, USA, 195 pp
14. Favre H (1935) Etude Théorique et Expérimentale des Ondes de Translation dans les Canaux Découverts. (Theoretical and experimental study of travelling surges in open channels). Dunod, Paris, France (in French)
15. Furuyama S, Chanson H (2008) A numerical study of open channel flow hydrodynamics and turbulence of the tidal bore and dam-break flows. Report no. CH66/08, Division of Civil Engineering, The University of Queensland, Brisbane, Australia, May, 88 pp
16. Goring DG, Nikora VI (2002) Despiking acoustic doppler velocimeter data. J Hydraul Eng ASCE 128(1):117–126 (discussion: 129(6):484–489)
17. Henderson FM (1966) Open channel flow. MacMillan Company, New York
18. Hinze JO (1973) Experimental investigation of secondary currents in the turbulent flow through a straight conduit. Appl Sci Res 28:453–465
19. Hornung HG, Willert C, Turner S (1995) The flow field downsteam of a hydraulic jump. J Fluid Mech 287:299–316
20. Kjerfve B, Ferreira HO (1993) Tidal bores: first ever measurements. Ciência e Cultura (J Brazilian Assoc Adv Sci) 45(2):135–138
21. Koch C, Chanson H (2008) Turbulent mixing beneath an undular bore front. J Coastal Res 24(4): 999–1007. doi:10.2112/06-0688.1
22. Koch C, Chanson H (2009) Turbulence measurements in positive surges and bores. J Hydraul Res IAHR 47(1): 29–40. doi:10.3826/jhr.2009.2954
23. Madsen PA, Simonsen HJ, Pan CH (2005) Numerical simulation of tidal bores and hydraulic jumps. Coastal Eng 52: 409–433. doi:10.1016/j.coastaleng.2004.12.007
24. Lemoine R (1948) Sur les Ondes Positives de Translation dans les Canaux et sur le Ressaut Ondulé de Faible Amplitude. (On the Positive Surges in Channels and on the Undular Jumps of Low Wave Height.) Jl La Houille Blanche, March–April, pp 183–185 (in French)
25. Liggett JA (1994) Fluid mechanics. McGraw-Hill, New York
26. Lubin P, Glockner S, Chanson H (2010) Numerical simulation of a weak breaking tidal bore. Mech Res Commun 37(1): 119–121. doi:10.1016/j.mechrescom.2009.09.008
27. Montes JS, Chanson H (1998) Characteristics of undular hydraulic jumps. Results and calculations. J Hydraul Eng ASCE 124(2):192–205
28. Peregrine DH (1966) Calculations of the development of an undular bore. J Fluid Mech 25:321–330
29. Rouse H (1938) Fluid mechanics for hydraulic engineers. McGraw-Hill Publ. New York (also 1961, Dover Publ., New York, 422 pp)
30. Rulifson RA, Tull KA (1999) Striped bass spawning in a tidal bore river: the Shubenacadie estuary, Atlantic Canada. Trans Am Fish Soc 128:613–624
31. Tessier B, Terwindt JHJ (1994) An example of soft-sediment deformations in an intertidal environment—the effect of a tidal bore. Comptes-Rendus de l'Académie des Sciences, Série II 319(2, Part 2):217–233 (in French)
32. Thorne CR, Hey RD (1979) Direct measurements of secondary currents at a river inflexion point. Nature 280(19):226–228
33. Trevethan M, Chanson H, Brown R (2008) Turbulence characteristics of a small subtropical estuary during and after some moderate rainfall. Estuar Coastal Shelf Sci 79(4): 661–670. doi:10.1016/j.ecss.2008.06.006

34. Wahl TL (2003) Despiking acoustic doppler velocimeter data. Discussion. J Hydural Eng ASCE 129(6):484–487
35. Wolanski E, Williams D, Spagnol S, Chanson H (2004) Undular tidal bore dynamics in the Daly estuary, Northern Australia. Estuar Coastal Shelf Sci 60(4): 629–636. doi:10.1016/j.ecss.2004.03.001
36. XIE Q (1998) Turbulent flows in non-uniform open channels: experimental measurements and numerical modelling. Ph.D. thesis, Department of Civil Engineering, University Of Queensland, Australia, 339 pp

DIGITAL APPENDIX

A series of short movies were further taken during the experiments. The Digital Files are a series of Quicktime™ movies.

Filename	Format	Description
10652_2010_9189_MOESM2_ESM.mov	Quicktime	Two-dimensional undular wave (Fr = 1.17) - Duration: 3 s. Run 090309_41, Q= 0.040 m^3/s, d_o = 0.179 m, S_o = 0, Fr = 1.17, U = 1.136 m/s.
10652_2010_9189_MOESM3_ESM.mov	Quicktime	Two-dimensional undular wave (Fr = 1.15) propagating (from right to left) between constriction - Duration: 9 s. Run 090318_00, Q= 0.0232 m^3/s, d_o = 0.155 m, S_o = 0, Fr = 1.15, U = 1.11 m/s.
10652_2010_9189_MOESM4_ESM.mov	Quicktime	Two-dimensional undular wave (Fr = 1.23) propagating between constriction, looking downstream - Duration: 6 s. Run 090324_00, Q= 0.0097 m^3/s, d_o = 0.0828 m, S_o = 0, Fr = 1.23, U = 0.885 m/s.
10652_2010_9189_MOESM5_ESM.mov	Quicktime	Two-dimensional undular wave (Fr = 1.23) propagating between constriction, looking upstream - Duration: 5 s. Run 090324_00, Q= 0.0097 m^3/s, d_o = 0.0828 m, S_o = 0, Fr = 1.23, U = 0.885 m/s.